

Physically Realizable Multi-User Radar/Communications (MURC)

Brandon Ravenscroft¹, Alfred Fontes¹, Patrick M. McCormick¹, Shannon D. Blunt¹, Cameron Musgrove²

¹Radar Systems Lab (RSL), University of Kansas (KU), Lawrence, KS

²IERUS Technologies, Inc., Huntsville, AL

Abstract—Leveraging a recent method for spectrally-shaped random FM (RFM) waveform generation, in conjunction with a particular implementation of spread-spectrum signaling, a multi-user form of dual-function radar/communication (DFRC) is proposed that seeks to balance the disparate requirements of each function. Using a radar-amenable spread-spectrum multiple-access signaling scheme, receive dynamic range for sensing is preserved by exploiting high-dimensional (and thus separable) waveforms, which are specifically structured to convey encoded information in a manner that can be readily decoded at a communication receiver.

Keywords—Dual-function radar/communications, multi-user, waveform diversity, spread spectrum

I. INTRODUCTION

Operation in congested spectral environments is, or will soon become, the norm for radar systems due to voracious demand for commercial wireless services. Consequently, radar systems will necessarily be tasked with performing spectrum sharing in some manner [1-4]. In short, the radar must consider interference both to and from other users in the environment.

In contrast to sharing spectrum between users, the prospect of realizing a dual-function radar/communication (DFRC) mode within a single system raises an altogether different design trade-space since the system retains complete control (as opposed to “external” users like commercial cellular), and yet must address the conflicting requirements of each function (e.g. [5-12]). For instance, the inherent signal variability that arises from conveying information also imposes a range sidelobe modulation (RSM) onto radar clutter that limits receiver sensitivity if it is not properly compensated [13-15].

Extending the DFRC concept from a single system to a network of multiple nodes introduces further complexity, while also beginning to blur the lines between spectrum sharing and DFRC (though here we only consider “internal” users in the form of other known radars). Put another way, can multiple proximate radars operate concurrently when each is using a DFRC mode? Moreover, can they do so without requiring additional spectrum resources, which are scarcely available, and without compromising their primary mission as a sensor?

Here we consider an approach to this multi-user radar/communication (MURC) problem that also accounts for the physical requirements of radar transmitters. Specifically, we examine the feasibility of a formulation possessing the following attributes: *a*) FM waveforms with sufficient spectral containment to be amenable to the radar transmitter; *b*) waveforms with high time-bandwidth product (TB) and

nonrepeating uniqueness to maximize separability on receive while also providing natural robustness to interference; and *c*) a communication encoding/decoding mechanism that is robust to multi-user interference while not degrading radar performance. Generally speaking, we leverage the merging of spread-spectrum (SS) multiple-access [16] with continuous phase modulation (CPM) [17] that previously realized SS/CPM [18-21]. In the context of continuous-wave (CW) radar, a minimum shift keying (MSK) instantiation of DFRC could conceivably be realized by direct application of [20], though adequate separability in each radar receiver would be lacking since the information-bearing symbols were represented by a reusable set of M codes (thus high dynamic range could not be achieved). Consequently, here we explore a DFRC-specific form that exploits the recent stochastic waveform generation (StoWGe) formulation from [22] as a means to realize a nonrepeating coding scheme with custom-designed spectrum shaping.

II. STOCHASTIC DFRC WAVEFORMS

As observed in [13], the trade-space that drives DFRC centers on the necessity for waveforms to possess a stochastic component that conveys information, with the modulation of radar clutter arising as a by-product. The StoWGe framework was developed as means to produce pulsed random FM (RFM) radar waveforms by converting a random discrete data stream into a continuously varying FM signal having desired attributes in the expectation [22]. Specifically, given a particular template for the desired power spectrum, a transform matrix was designed via gradient-based optimization such that a Gaussian random process with zero-mean and unit variance would realize an FM signal adhering to the desired template on average.

The combination of FM structure and proper choice of template (for sufficient spectral containment) makes StoWGe waveforms naturally amenable to the high-power amplification in radar transmitters. Further, since the transform matrix design only needs to occur once for a given template, an unlimited supply of unique, pulsed RFM waveforms can be generated. For pulse width T and 3-dB bandwidth B (set by the template), each waveform constitutes an FM signal of time-bandwidth product TB and possesses a unique continuous phase trajectory.

In [23], a continuous-wave (CW) version of StoWGe was defined along with the consideration of driving this discrete-to-continuous mapping with various non-Gaussian distributions. A notable consequence of this CW form is a structural simplification that can be viewed as using StoWGe to design the shaping filter in the CPM context [17] to yield a desired spectral response. A nonlinear communication modulation, CPM is used

extensively in aeronautical telemetry [24] and has also been modified to enable conversion of arbitrary polyphase radar codes into physically realizable FM waveforms [25]. Here we leverage the CW version of StoWGe in [23] that operates on a random binary distribution to pose the SS/CPM concept from [20] as a multi-user form of DFRC.

III. BRIEF REVIEW OF CPM COMMUNICATIONS

Standard CPM maps the communication symbol stream $\beta[m]$, taken from a pulse amplitude modulation (PAM) constellation $\{\pm 1, \pm 3, \dots\}$ for symbol index m , into a digital FM signal. As the first step in this process, the symbols are mapped onto the continuous-time weighted impulse train

$$\sum_m \beta[m] \delta(\tau - mT_s), \quad (1)$$

where T_s is the inter-symbol spacing. This weighted impulse train is convolved with frequency shaping filter $b(\tau)$ to obtain

$$\sum_m \beta[m] b(\tau - mT_s), \quad (2)$$

where $b(\tau)$ integrates to $\frac{1}{2}$ and is only non-zero for the time interval $0 \leq t \leq LT_s$, with L an integer known as the partial response parameter. Setting $L = 1$ indicates full-response CPM, while $L > 1$ denotes partial response CPM [26]. The filtered result of (2) is then integrated to form the phase function

$$\theta(t; \mathbf{\beta}) = 2\pi h \int_0^t \left[\sum_m \beta[m] b(\tau - mT_s) \right] d\tau, \quad (3)$$

in which h is the modulation index [17] that dictates the rate of phase change (and therefore scales the spectral content) and $\mathbf{\beta}$ is the collection of symbols. Finally, the phase function is exponentiated to produce the CPM waveform

$$s(t; \mathbf{\beta}) = \exp\{j(\theta(t; \mathbf{\beta}))\}, \quad (4)$$

with the combination of the shaping filter, integration, and exponentiation yielding an FM structure that is constant amplitude and phase-continuous.

IV. STOUGE-BASED SS/CPM

For the communication-only application, typical shaping filters $b(t)$ used in CPM include rectangular, raised-cosine, and others. In the DFRC context, however, we must pay particular attention to the shape of the power spectral density (PSD) because the Fourier-related autocorrelation determines the range sidelobe response; hence the utility of CW-StoWGe to realize a custom-designed PSD.

The StoWGe-SS/CPM arrangement involves some other changes as well. Each symbol $\beta[m]$ of the information-bearing data stream in (1) is now modulated by a group of N chip values to spread the symbol information in frequency. Define the m th $N \times 1$ code segment corresponding to the m th symbol $\beta[m]$ as \mathbf{a}_m , where each code value $a_m[n]$ is drawn randomly from the discrete bivariate distribution $\{-1, 1\}$ so that \mathbf{a}_m is unique from symbol to symbol. Therefore, the product $\beta[m]\mathbf{a}_m$ represents a sequence of N chip values encoded with symbol information that can be implemented in the CPM modulation framework from Sect. III with a chip spacing of $T_c = T_s/N$. Since $\beta[m]$ is drawn from a symmetric PAM constellation, the product with a

bivariate \mathbf{a}_m does not alter the symbol distribution. Here, we consider one bit per symbol, so $\beta[m] \in \{-1, 1\}$, and therefore $\beta[m]\mathbf{a}_m$ is likewise drawn from a bivariate distribution, which has been shown [23] to provide the best spectral match when designing StoWGe shaping filter $b(t)$ according to a desired spectral template [22].

The frequency shaping filter $b(t)$ is optimized using StoWGe's expected frequency template error (ETFE) objective function [22] so that the waveform conforms to a desired PSD for a given chip duration T_c . The resulting shaping filter is denoted $b_s(t; L, \eta)$, which depends on a prescribed partial response parameter L (here always > 1) and η is the super-Gaussian template spectral exponent described in [27,28] that controls containment. In contrast to standard CPM, the CW-StoWGe filter generally does not integrate to $\frac{1}{2}$ and cannot simply be normalized to do so without altering the optimized behavior of the filter. Moreover, the StoWGe-SS/CPM framework does not use modulation index h because scaling is addressed by the shaping filter optimization. For example, Fig. 1 illustrates the CW-StoWGe filter designed for $L = 8$ and $\eta = 4$, where the optimization has produced a rather more complicated structure than the standard CPM filters (rectangular (RECT) and raised-cosine (RC)) that are also depicted. Note that the partial response parameter L is defined relative to the chip duration T_c (for CW-StoWGe) and not the symbol duration T_s .

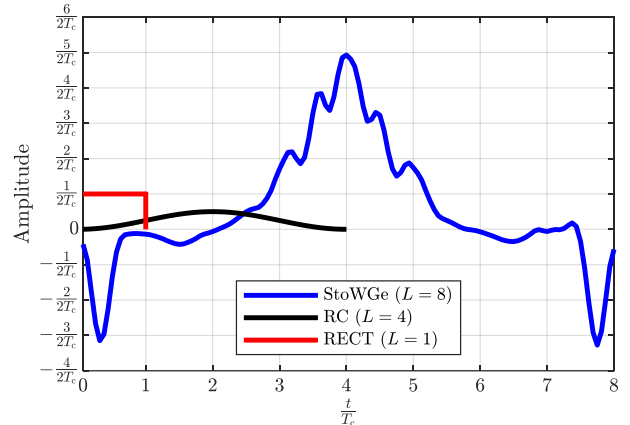


Fig. 1: Optimized CW-StoWGe shaping filter (blue) compared to standard rectangular (red) and raised-cosine (black)

Incorporating these changes into the CPM framework yields the StoWGe-SS/CPM waveform, which takes the form

$$s(t) = \exp\left\{j\left(\pi \int_0^t \left[\sum_m \beta[m] \sum_{n=0}^{N-1} a_m[n] b_s(\tau - nT_c - mT_s) \right] d\tau \right)\right\} \quad (5)$$

with parameter dependencies excluded for brevity. While (5) appears similar to the combination of (3) and (4), some important distinctions bear consideration. The SS coding can be generated using a pseudo-random noise (PRN) sequence that is effectively nonrepeating. The always changing N -length \mathbf{a}_m code segments can thus be known by a desired receiver that possesses the same PRN generator function and initial/current state. Moreover, the underlying PRN structure, mapped through the StoWGe-SS/CPM implementation, provides a natural multi-user DFRC capability that is amenable to radar transmitters, can be decoded by communication receivers via appropriate

sequence matching, and can achieve high dynamic range for radar receivers. The latter arises because unique emitter signals do not repeat (effectively) and thus realize high dimensionality (high TB), where sidelobe suppression and separability from other signals are on the order of $10 \log_{10}(TB)$ [29].

The MURC framework therefore involves the use of $k = 1, 2, \dots, K$ emitters producing the distinct signals

$$s_k(t) = \exp \left\{ j \left(\pi \int_0^t \left[\sum_m \beta_k[m] \sum_{n=0}^{N-1} \alpha_{m,k}[n] b_s(\tau - nT_c - mT_s) \right] d\tau \right) \right\} \quad (6)$$

that are each parameterized by unique data stream $\beta_k[m]$ and uniquely identifying code $\alpha_{m,k}[n]$. It is knowledge of the latter that permits the intended communication receiver to extract the data stream from a superposition of these FM signals (corrupted by noise, multipath, and possibly other interference), while each signal itself remains a useful CW radar waveform due to the imposed spectral shaping and physical structure.

As a point of comparison, (6) can also be used to implement a direct-sequence SS form of minimum shift keying (MSK) [30] simply by replacing the CW-StoWGe filter $b_s(t; L, \eta)$ with the rectangular filter from Fig. 1 for which $L = 1$. We shall refer to this version as MSK-SS/CPM. The subsequent radar or communication receive processing remains the same.

V. RADAR RECEIVE PROCESSING

Radar receive processing can be readily performed using the signal from any of the emitters. At the i th radar receiver we can express the incident signal as

$$y_i(t) = \sum_{k=0}^{K-1} s_k(t) * x_{k,i}(t) + v_i(t), \quad (7)$$

where $x_{k,i}(t)$ is the scattering induced by waveform $s_k(t)$ and captured at the i th receiver, inclusive of the corresponding transmit/receive beamforming and relative geographical arrangement, and with additive noise $v_i(t)$. Since each $x_{k,i}(t)$ profile can also subsume direct-path leakage between a given transmit/receive pair, the model in (7) denotes the totality of “internal” interference that a given radar receiver experiences.

Assuming each radar is operating independently as a monostatic sensor, then the i th radar must rely on the $y_i(t)$ superposition in (7) to estimate the scattering $x_{(k=i),i}(t)$ induced by illumination $s_{(k=i)}(t)$. For independent waveforms and scattering across emitters, this estimation is accomplished by coherent matching to the desired waveform $s_i(t)$ while the other $K - 1$ components establish the interference floor.

Divide the i th CW signal into arbitrary-length waveform sections of extent T_{sect} (i.e. not dependent on α code segment extent) in a manner such that contiguous sections possess sufficient overlap to account for convolutional tails when applied as a pulse compression matched filter (see [31,32]). The resulting sequence of range domain responses can then be Doppler processed in the usual manner. Per [31,32], direct-path leakage for the i th collocated transmitter/receiver can be addressed using a form of the CLEAN algorithm (e.g. [33]).

Reasonable separability from the other $K - 1$ scattering components arises from the assumption that each CW signal has a high TB . As noted above and illustrated in the next section, the separability of two signals occupying the same

spectrum at the same time is on the order of $10 \log_{10}(TB)$. For instance, for two signals having 100 MHz (10^8) bandwidth and a receive time interval of 10 ms (10^{-2}), then $TB = 10^6$ and they achieve a separability of ~ 60 dB if completely unique.

VI. COMMUNICATION RECEIVE PROCESSING

Extraction of encoded information from the k th emitter at some intended communication receiver is similar to radar processing, with the exception that the actual transmitted signal is hypothesized instead of being known exactly. Put another way, this receiver possesses knowledge of the underlying PRN sequence that produces α_m code segments, but the $\beta[m]$ symbol sequence is unknown information for the receiver to decode.

Let the superimposed signal at the intended receiver be

$$y_c(t) = \sum_{k=0}^{K-1} s_k(t) * x_{c,k}(t) + v_c(t), \quad (8)$$

where $x_{c,k}(t)$ is the multipath scattering of waveform $s_k(t)$ as observed by the communication receiver and $v_c(t)$ is additive noise. Since we are assuming this receiver has knowledge of α_m , it is likewise reasonable to assume at least modest transmit/receive synchronization. Consequently, let $\bar{y}_c^{(m)}(t)$ be a portion of the signal in (8) that sufficiently encompasses the interval of the m th code segment (corresponding to the m th symbol), with some excess before/after for timing error tolerance.

Decoding then involves the pair of hypothesized signals

$$s_{k,+1}^{(m)}(t) = \exp \left\{ j \left(\pi \int_0^t \left[(+1) \sum_{n=0}^{N-1} \alpha_{m,k}[n] b_s(\tau - nT_c) \right] d\tau \right) \right\} \quad (9)$$

and

$$s_{k,-1}^{(m)}(t) = \exp \left\{ j \left(\pi \int_0^t \left[(-1) \sum_{n=0}^{N-1} \alpha_{m,k}[n] b_s(\tau - nT_c) \right] d\tau \right) \right\} \quad (10)$$

for the k th emitter and for each α_m code segment, with (9) and (10) clearly the complex conjugate of one another. While the binary code/symbol framework might appear to cause these signals to be identical (aside from a sign difference), the filtering and integration stages produce continuous-phase trajectories that are distinct and likewise achieve separability on the order of $10 \log_{10}(T_s B)$. Fig. 2 depicts a random instantiation with $T_s B = 100$, which in this case yields a peak cross-correlation of about -15 dB.

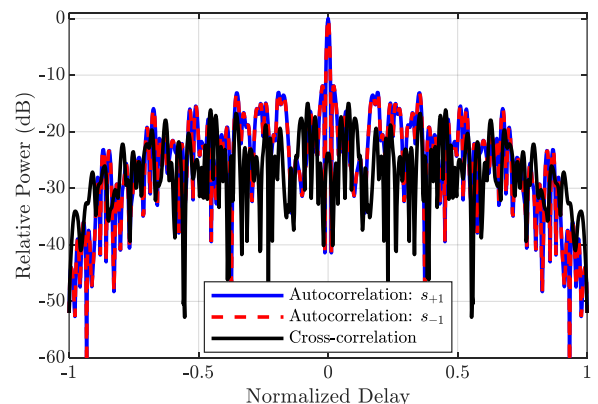


Fig. 2: Example hypothesized signals from (9) and (10) for $T_s B = 100$ depicting autocorrelations (i.e. coherently matched to received signal) and cross-correlation (the dissimilarity between coded symbols)

We can therefore pose the decoding hypothesis test

$$\left(\max_i \left| h_{k+1}^{(m)}(t) * \bar{y}_c^{(m)}(t) \right| \right)_{H_{+1}} > \left(\max_i \left| h_{k-1}^{(m)}(t) * \bar{y}_c^{(m)}(t) \right| \right)_{H_{-1}} \quad (11)$$

with $h_{k+1}^{(m)}(t) = (s_{k+1}^{(m)}(-t))^*$ and $h_{k-1}^{(m)}(t) = (s_{k-1}^{(m)}(-t))^*$ the matched filters. Distinct from the “code as symbol” form of [20], which involved a fixed set of codes for each user, here the m th symbol for the k th emitter produces a pair of filters that naturally separate via their complex conjugate relationship and are perpetually replaced with new versions.

Note that $2K$ filters are needed to decode all K concurrent symbols, with each emitter driven by a different PRN sequence. The decoding in (11) makes no assumption about the K concurrent symbols being synchronous, only that the timing of a particular desired code segment is adequately known. Finally, one could conceivably perform multipath combining by replacing the $\max(\cdot)$ operations in (11) with summations, which should further improve symbol estimation performance.

VII. SIMULATION RESULTS (RADAR ANALYSIS)

Consider StoWGe and MSK (for comparison) versions of the proposed SS/CPM framework for DFRC using the shaping filters from Fig. 1 (rectangular for MSK). For total $TB = 4 \times 10^5$, unique CW waveforms were generated for each case, with Fig. 3 illustrating the resulting power spectrum along with desired template. The MSK spectrum clearly takes the shape one expects [17], exhibiting a gradual roll-off that may violate the radar’s spectral containment mask while also incurring greater transmitter distortion. In contrast, the StoWGe spectrum follows the desired template down to nearly -40 dB (from the normalized peak) and thereafter yields a flat roll-off more than 10 dB lower than MSK.

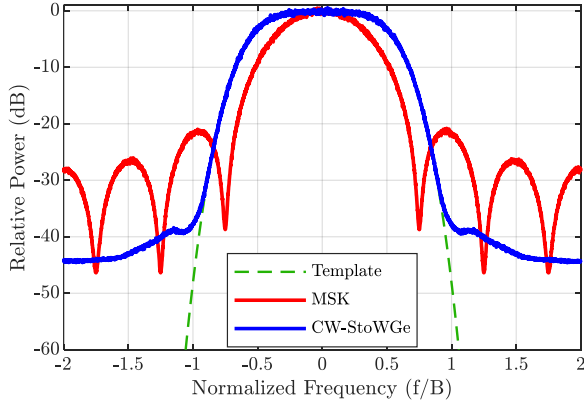


Fig. 3: Spectrum plot showing CW-StoWGe optimization template (green), the resulting CW-StoWGe power spectrum estimate (blue), and MSK power spectrum estimate (red)

To assess section-wise radar receive processing, each CW waveform was divided into 400 sections, with each section having a time-bandwidth product of $T_{\text{sect}}B = 10^3$. Consequently, it is not surprising that the root-mean square (RMS) average of the section-wise autocorrelations in Fig. 4 yields a sidelobe response that is almost exactly $-10 \log_{10}(T_{\text{sect}}B) = -30$ dB. Moreover, subsequent slow-time coherent combining (i.e. Doppler processing) across the 400 unique sections (without

RMS averaging) is expected to provide an additional $10 \log_{10}(400) = 26$ dB of sidelobe suppression, which agrees with the “Mean” result in Fig. 4.

Fig. 5 shows a close-up view of the respective mainlobe responses from Fig. 4. Of particular note are the “shoulder” lobes for CW-StoWGe, which arise from the $\eta = 4$ super-Gaussian spectral shape to which the signal is designed [27,28]. These shoulder lobes can simply be viewed as an extension of the mainlobe, with StoWGe also realizing a 2 dB lower sidelobe floor on top of the benefits of improved spectral containment.

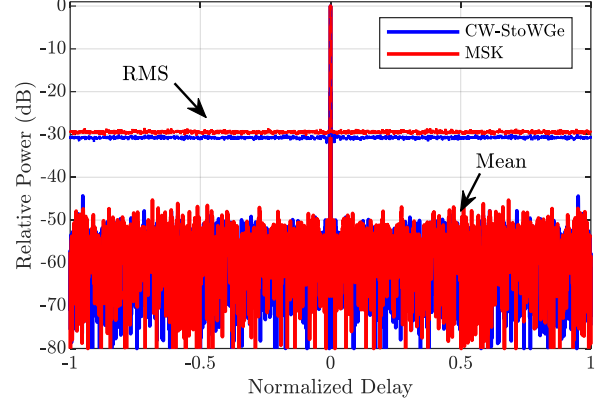


Fig. 4: RMS and mean (coherent) autocorrelation of CW-StoWGe (blue) and MSK (red) for total $TB = 4 \times 10^5$ and 400 segments

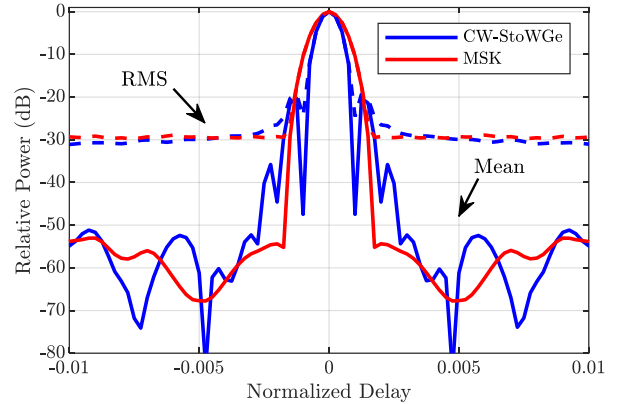


Fig. 5: Mainlobe detail of RMS and mean (coherent) autocorrelation of CW-StoWGe (blue) and MSK (red) for total $TB = 4 \times 10^5$ and 400 segments

The nonrepeating nature of these CW signals has the further utility of effectively eliminating range ambiguities, which is shown by examining the cross-correlation between contiguous segment pairs (see Fig. 6). The RMS and coherent mean sidelobe levels here are identical to those in Fig. 4. Further, assuming a set of K radars use CW-StoWGe or MSK signal structures, uniquely produced by each emitter, then the response in Fig. 6 illustrates the emitter-to-emitter cross-correlation one can expect for a given pair. The linear superposition in (7) also means that the cross-correlation floor one would expect from the $K-1$ other emitters is simply $10 \log_{10}(K-1)$ higher than the response in Fig. 6 (assuming the same bandwidths and general signal structures).

Finally, Figs. 7 and 8 depict the radar point spread function (PSF) for each waveform based on the same manner of sectioning, with pulse compression and subsequent slow-time

processing across sections. Doppler sidelobes could readily be reduced via standard tapering but has not been applied here. As expected from Fig. 5, CW-StoWGe has a narrower mainlobe in range (along with visible shoulder lobes) arising from the different spectral shape/width. Away from the mainlobe and Doppler roll-off, we observe that CW-StoWGe exhibits a delay/Doppler background that appears slightly lower (is actually 1.3 dB lower), which will translate into a similarly lower amount of clutter RSM [13-15].

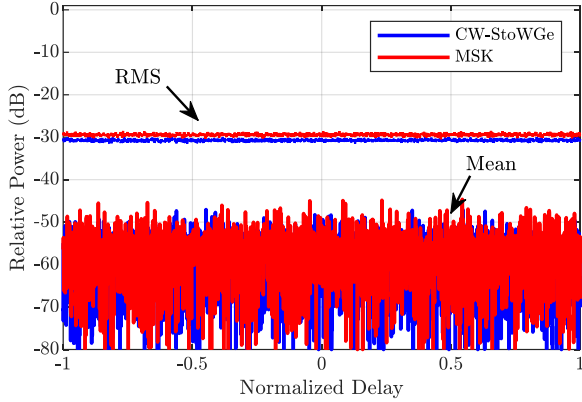


Fig. 6: RMS and mean (coherent) cross-correlation of CW-StoWGe (blue) and MSK (red) for total $T_s B = 4 \times 10^5$ and 400 segments

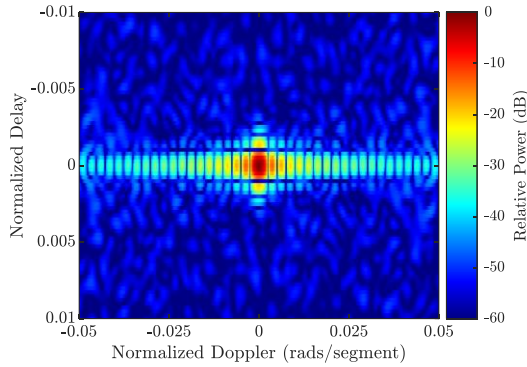


Fig. 7: Mainlobe detail view of point spread function for CW-StoWGe based on segments of $T_{\text{sect}} B = 10^3$

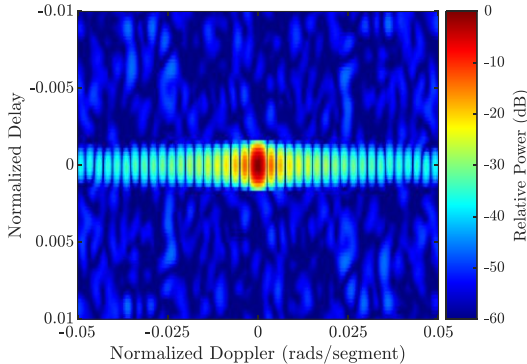


Fig. 8: Mainlobe detail view of point spread function for MSK based on segments of $T_{\text{sect}} B = 10^3$

VIII. SIMULATION RESULTS (COMMUNICATION ANALYSIS)

Because both the coding $\alpha[n]$ and symbol stream $\beta[m]$ are random binary processes, the particular code length N and ensuing per-symbol time-bandwidth product (denoted $T_s B$)

have no impact on radar performance. Clearly, these parameters do affect communication data rate and symbol error rate (SER).

For values of $T_s B$ set to 20, 40, 60, 80 and 100, we examine the decoding procedure described in (8)-(11). For a 3-dB bandwidth of 50 MHz, these values translate to data rates of 2.5, 1.25, 0.83, 0.63 and 0.50 Mb/s, respectively (for 1 bit/symbol). Varying the number of emitters from $k = 1, 2, \dots, 10$, Monte Carlo simulations were performed for 10^4 independent trials.

For the sake of simplicity, the communication channels were assumed to only possess a direct path component (i.e. no multipath) and no “near/far” disparity between received signal powers was considered. Finally, no additive noise was included. In short, the following conveys a simplified analysis to isolate a performance comparison due solely to multi-user interference, with considerable trade-offs, practical effects, and experimental assessment remaining to be examined (in sequel work).

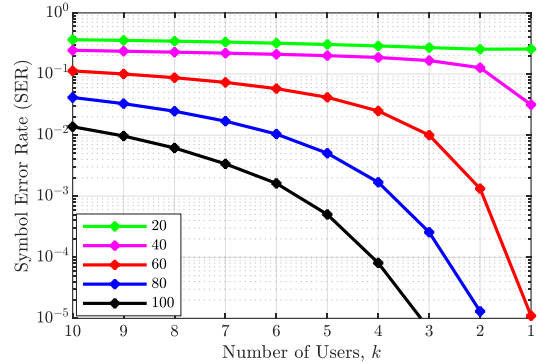


Fig. 9: CW-StoWGe SER plot for 10^4 Monte Carlo trials for various per-symbol time-bandwidth products $T_s B$

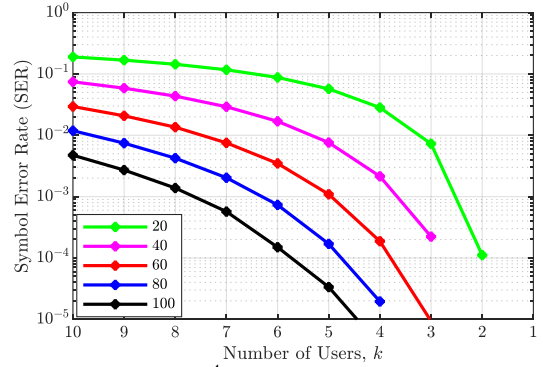


Fig. 10: MSK SER plot for 10^4 Monte Carlo trials for various per-symbol time-bandwidth products $T_s B$

Figs. 9 and 10 depict the resulting Monte Carlo SER curves for CW-StoWGe and MSK, respectively. As expected, there is a clear trend toward better estimation performance (lower SER) as the $T_s B$ devoted to each symbol increases, which in turn yields a lower data rate. We also see that MSK is clearly outperforming CW-StoWGe, which is not surprising since the $L = 1$ full response shaping filter of the former naturally avoids inter-symbol interference (ISI) in the absence of multipath. Indeed, MSK can achieve perfect decoding for the $k = 1$ case due to the complete absence of noise and multipath.

In contrast, the $L = 8$ partial response shaping filter that allows StoWGe to achieve desirable spectrum shaping for radar is somewhat detrimental to the communication function, with

even the $k = 1$ case exhibiting decoding errors (especially when $T_s B$ is low). However, there is clearly a regime of high enough $T_s B$ and low enough K where acceptable performance is possible, though this result does suggest the need for further investigation into whether StoWGe filter optimization can also account for SER performance. Note that the demodulator used here is simple and does not address ISI caused by the CW-StoWGe partial response shaping filter. At the cost of higher complexity, more sophisticated extensions of (9)-(11) could conceivably address ISI as well as incorporate error correction.

IX. CONCLUSIONS

A framework for multi-user DFRC operation has been proposed with a goal of addressing the rigors of high-power radar transmitters and realizing sufficient radar receive separability. Being based on random binary coding and data, mapped into a physical FM signal structure possessing good spectral containment, the resulting nonrepeating CW signal is easily scalable according to desired data rate and number of concurrent emitters. Compared to MSK as a baseline, the CW-StoWGe form does exhibit poorer communication performance as part of the trade-off for better spectral containment and marginally better radar performance, though further work is needed to fully explore this trade-space.

REFERENCES

- [1] H. Griffiths, L. Cohen, S. Watts, E. Mokole, C. Baker, M. Wicks, S. Blunt, "Radar spectrum engineering and management: technical and regulatory issues," *Proc. IEEE*, vol. 103, no. 1, pp. 85-102, Jan. 2015.
- [2] A. Martone, M. Amin, "A view on radar and communication systems coexistence and dual functionality in the era of spectrum sensing," *Digital Signal Processing*, June 2021.
- [3] S.D. Blunt, E.S. Perrins, eds., *Radar & Communication Spectrum Sharing*, SciTech Publishing, 2018.
- [4] J. Owen, C. Mohr, B. Ravenscroft, S. Blunt, B. Kirk, A. Martone, "Real-time experimental demonstration and evaluation of open-air sense-and-notch radar," *IEEE Radar Conf.*, New York City, NY, Mar. 2022.
- [5] P.M. McCormick, S.D. Blunt, J.G. Metcalf, "Simultaneous radar and communications emissions from a common aperture, part I: theory," *IEEE Radar Conf.*, Seattle, WA, May 2017.
- [6] P.M. McCormick, B. Ravenscroft, S.D. Blunt, A.J. Duly, J.G. Metcalf, "Simultaneous radar and communication emissions from a common aperture, part II: experimentation," *IEEE Radar Conf.*, Seattle, WA, May 2017.
- [7] A. Hassanien, B. Himed, B.D. Rigling, "A dual-function MIMO radar-communications system using frequency-hopping waveforms," *IEEE Radar Conf.*, Seattle, WA, May 2017.
- [8] C. Sahin, J. Jakabosky, P.M. McCormick, J.G. Metcalf, S.D. Blunt, "A novel approach for embedding communication symbols into physical radar waveforms," *IEEE Radar Conf.*, Seattle, WA, May 2017.
- [9] B. Ravenscroft, P.M. McCormick, S.D. Blunt, E. Perrins, J.G. Metcalf, "A power-efficient formulation of tandem-hopped radar & communications," *IEEE Radar Conf.*, Oklahoma City, OK, Apr. 2018.
- [10] C. Sahin, J. G. Metcalf, A. Kordik, T. Kendo, T. Corigliano, "Experimental validation of phase-attached radar/communication (PARC) waveforms: radar performance," *Intl. Conf. Radar*, Brisbane, Australia, Aug. 2018.
- [11] B. Ravenscroft, P. McCormick, S. Blunt, E. Perrins, C. Sahin, J. Metcalf, "Experimental assessment of tandem-hopped radar and communications (THoRaCs)," *Intl. Radar Conf.*, Toulon, France, Sept. 2019.
- [12] A.C. O'Connor, D.J. Rabideau, "Dual-beam transmit from shared aperture with constant envelope constraint," *IEEE Radar Conf.*, Boston, MA, Apr. 2019.
- [13] S.D. Blunt, M.R. Cook, J. Stiles, "Embedding information into radar emissions via waveform implementation," *Intl. Waveform Diversity & Design Conf.*, Niagara Falls, Canada, Aug. 2010.
- [14] B. Ravenscroft, J.W. Owen, B.H. Kirk, S.D. Blunt, A.F. Martone, K.D. Sherbondy, R.M. Narayanan, "Experimental assessment of joint range-Doppler processing to address clutter modulation from dynamic radar spectrum sharing," *IEEE Intl. Radar Conf.*, Washington, DC, Apr. 2020.
- [15] C. Jones, B. Ravenscroft, J. Vogel, S.M. Shontz, T. Higgins, K. Wagner, S. Blunt, "Computationally efficient joint-domain clutter cancellation for waveform-agile radar," *IEEE Radar Conf.*, Atlanta, GA, May 2021.
- [16] D. Torrieri, *Principles of Spread-Spectrum Communication Systems*, vol. 5. Springer, 2022.
- [17] J.B. Anderson, T. Aulin, C. Sundberg, *Digital Phase Modulation*. Plenum Press, 1986.
- [18] A.T. McDowell, J.S. Lehnert, "Phase-independent continuous phase modulation for bandwidth efficient multiple-access communication," *IEEE Military Comm. Conf.*, San Diego, CA, Oct. 1992.
- [19] A.T. McDowell, J.S. Lehnert, Y.K. Jeong, "Dual-phase continuous phase modulation for spread-spectrum multiple-access communication," in *IEEE Transactions on Communications*, vol. 52, no. 5, pp. 823-833, May 2004.
- [20] T.M. Lok, J.S. Lehnert, "DS/SSMA communication system with trellis coding and CPM," *IEEE J. Selected Areas Comm.*, vol. 12, no. 4, pp. 716-722, May 1994.
- [21] N. Mazzali, G. Colavolpe, S. Buzzi, "CPM-based spread spectrum systems for multi-user communications," *IEEE Trans. Wireless Comm.*, vol. 12, no. 1, pp. 358-367, Jan. 2013.
- [22] C.A. Mohr, S.D. Blunt, "Design and generation of stochastically defined, pulsed FM noise waveforms," *Intl. Radar Conf.*, Toulon, France, Sept. 2019.
- [23] C.A. Mohr, "Design and evaluation of stochastic processes as physical radar waveforms," PhD dissertation, University of Kansas, June 2021.
- [24] Range Commanders Council Telemetry Group. IRIG standard 106-20: Telemetry Standards. White Sands Missile Range, NM, Jul. 2020.
- [25] S. Blunt, M. Cook, J. Jakabosky, J. De Graaf, E. Perrins, "Polyphase-coded FM (PCFM) radar waveforms, part I: implementation," *IEEE Trans. Aerospace & Electronic Systems*, vol. 50, no. 3, pp. 2218-2229, July 2014.
- [26] J. Proakis, M. Salehi, *Digital Communications*, vol. 4. McGraw-Hill, 2001.
- [27] C.A. Mohr, S.D. Blunt, "Designing random FM radar waveforms with compact spectrum," *IEEE Intl. Conf. Acoustics, Speech & Signal Processing*, Toronto, Canada, June 2021.
- [28] M.B. Heintzelman, T.J. Kramer, S.D. Blunt, "Experimental evaluation of super-Gaussian-shaped random FM waveforms," *IEEE Radar Conf.*, New York City, NY, Mar. 2022.
- [29] S.D. Blunt, *et al.*, "Principles and applications of random FM radar waveform design," *IEEE Aerospace & Electronic Systems Mag.*, vol. 35, no. 10, pp. 20-28, Oct. 2020.
- [30] S. Pasupathy, "Minimum shift keying: A spectrally efficient modulation," *IEEE Comm. Mag.*, vol. 17, no. 4, pp. 14-22, July 1979.
- [31] J. Jakabosky, S.D. Blunt, B. Himed, "Waveform design and receive processing for nonrecurrent nonlinear FMCW radar," *IEEE Intl. Radar Conf.*, Washington, DC, May 2015.
- [32] T.J. Kramer, E.R. Biehl, M.B. Heintzelman, S.D. Blunt, E.D. Steinbach, "Compact parameterization of nonrepeating FMCW radar waveforms," *IEEE Radar Conf.*, San Antonio, TX, May 2023.
- [33] K. Kulpa, "The CLEAN type algorithms for radar signal processing," *Microwaves, Radar & Remote Sensing Symp.*, Kiev, Ukraine, Sept. 2008.